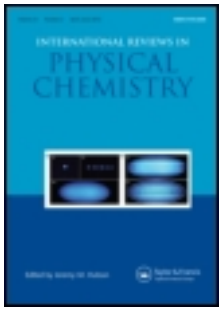

International Reviews in Physical Chemistry

Publication details, including instructions for authors and subscription information:
http://www.tandfonline.com/loi/trpc20

Coulomb-crystallised molecular ions in traps: methods, applications, prospects

Stefan Willitsch [a]

[a] Department of Chemistry , University of Basel , Klingelbergstrasse 80 , Basel 4056 , Switzerland

Published online: 27 Mar 2012.

To cite this article: Stefan Willitsch (2012) Coulomb-crystallised molecular ions in traps: methods, applications, prospects, International Reviews in Physical Chemistry, 31:2, 175-199, DOI: 10.1080/0144235X.2012.667221

To link to this article: http://dx.doi.org/10.1080/0144235X.2012.667221

International Reviews in Physical Chemistry
Vol. 31, No. 2, April–June 2012, 175–199

Taylor & Francis
Taylor & Francis Group

Coulomb-crystallised molecular ions in traps: methods, applications, prospects

Stefan Willitsch*

Department of Chemistry, University of Basel, Klingelbergstrasse 80, Basel 4056, Switzerland

(*Received 22 December 2011; final version received 13 February 2012*)

Translationally cold, spatially localised molecular ions prepared by sympathetic cooling with laser-cooled atomic ions in ion traps have recently found a wide range of applications in both chemistry and physics. The very low temperatures of the ions (down to millikelvins), their tight localisation in the trap and the ability to control and manipulate single isolated molecules on the quantum level offer intriguing possibilities for new experiments in the realms of cold chemistry, precision molecular spectroscopy, mass spectrometry and quantum technology. The present article gives an overview of the basic experimental methods, current topics and recent developments in this field.

Keywords: Coulomb crystals; molecular ions; ion traps; sympathetic cooling; cold molecules; cold chemistry; precision spectroscopy

Contents

*Email: stefan.willitsch@unibas.ch

ISSN 0144–235X print/ISSN 1366–591X online

http://dx.doi.org/10.1080/0144235X.2012.667221
http://www.tandfonline.com

1. Introduction

Ordered structures of translationally cold molecular ions in ion traps, usually referred to as 'Coulomb crystals', represent an unusual form of matter which has found a range of intriguing applications in both physics and chemistry over the past few years [1–3]. Coulomb crystals can be generated by confining molecular ions in an ion trap and cooling their translational motion sympathetically to millikelvin temperatures using the interaction with simultaneously trapped laser-cooled atomic ions. Under these conditions, the ions localise in the trap so that it is possible to observe, address and manipulate single particles. Experiments are carried out in an ultrahigh-vacuum chamber in which collisions and other perturbations from the surroundings are efficiently suppressed. Apart from the trapping fields, the only major interaction with the environment is the radiative coupling to the ambient black-body radiation field.

These intriguing features of Coulomb-crystallised molecular ions set the stage for a range of fascinating applications such as studies of chemical reactions at extremely low temperatures with single ions, spectroscopic precision measurements and the manipulation of single molecules on the quantum level. As becomes evident from these examples, research on cold molecular ions is highly interdisciplinary and bridges the boundaries between various established fields such as ultralow-temperature physics, plasma physics, chemical reaction dynamics, molecular spectroscopy and quantum information.

The topic has been reviewed previously with the most recent overview articles covering the developments up to 2008 [1–3]. However, the field has been progressing fast since then and recent advances have opened up several new research directions and perspectives. Following a summary of the basic concepts and methods used in ion trapping and cooling, the current article gives an overview of the most recent developments in the field. Topics discussed in previous reviews will only be mentioned briefly for completeness.

2. Ion trapping and cooling

Although Coulomb crystallisation of ions has also been studied in Penning traps, see, e.g., Refs. [4–7], the vast majority of experiments have been carried out in linear-quadrupole radio-frequency (RF) traps.

2.1. *Linear-quadrupole radio-frequency ion traps*

The theory of RF ion traps and the laser cooling of ions in these devices has extensively been treated in textbooks and previous reviews, see, e.g., Refs.[1–3,8–15]. The traps

conventionally used for the laser- and sympathetic cooling of ions are linear-quadrupole traps (also referred to as linear Paul traps) [2,11,16–18]. A generic linear Paul trap (shown in Figure 1(a)) consists of four cylindrical electrodes broken down into several segments to which static and time-varying voltages in the RF domain are applied.

Because Earnshaw's theorem forbids the generation of a static electric potential minimum, RF fields are used to trap the ions dynamically. The time-varying fields are generated by applying voltages $V_{\mathrm{RF}}(t) = V_0 \cos(\Omega_{\mathrm{RF}} t)$ with opposite polarity across neighbouring electrodes as indicated in Figure 1(a). Here, V_0 is the RF amplitude, Ω_{RF} is the angular frequency and t is the time. As a result, an oscillating potential saddle point is created which traps the ions dynamically in the (x, y) plane perpendicular to the trap axis. In the direction along the axis (z), the ions are confined using static potentials V_{END} applied to the 'endcap' electrodes of the trap.

In a linear Paul trap, the electrodes are arranged to generate an almost ideal quadrupolar electric potential close to the trap centre [8,12,13]. The trajectory of a single ion in the trap can be obtained analytically from the solution of the Mathieu equations

$$\frac{d^2u}{dt^2} + \frac{\Omega_{\mathrm{RF}}^2}{4}\left(a_u + 2q_u \cos(\Omega_{\mathrm{RF}} t)\right)u = 0, \tag{1}$$

where $u \in \{x, y, z\}$. Stable trapping of the ion is only achieved for specific values of the Mathieu parameters a_u and q_u which are defined by[1]

$$\begin{aligned} a_x = a_y = -\frac{1}{2}a_z = -\kappa\frac{4QV_{\mathrm{END}}}{m\Omega_{\mathrm{RF}}^2 z_0^2}, \\ q_x = -q_y = \frac{4QV_0}{m\Omega_{\mathrm{RF}}^2 r_0^2}, \quad q_z = 0. \end{aligned} \tag{2}$$

In Equations (2), m and Q stand for the mass and the charge of the ion, respectively, $2z_0$ is the distance between the endcaps, κ is a geometry parameter, and $2r_0$ is the distance between two diagonally opposed quadrupole rods (see Figure 1(a)). The regions for stable confinement in a_u, q_u space are usually represented in terms of stability diagrams, see e.g., Refs. [11–13,18].

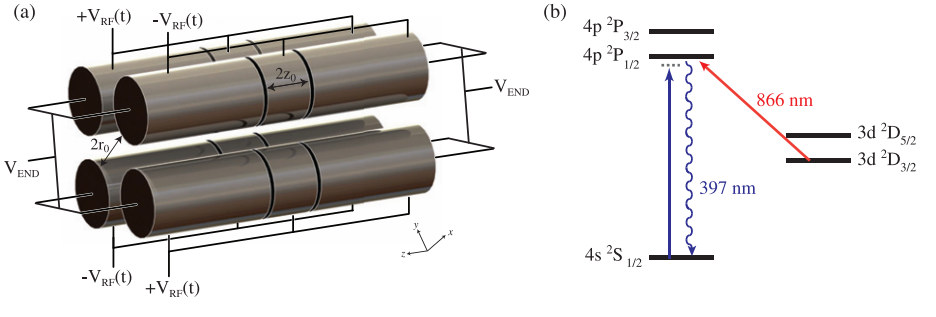

Figure 1. (Colour online) (a) Schematic representation of a linear Paul trap following the design of Ref. [11]. Ions are confined in the centre of the trap by applying radio-frequency voltages $V_{\mathrm{RF}}(t)$ and static voltages V_{END} to the electrodes as indicated. (b) Energy-level scheme for the Doppler laser cooling of $^{40}Ca^+$ ions. Cooling is achieved by repeatedly exciting the $4s\ ^2S_{1/2} \rightarrow 4p\ ^2P_{1/2}$ transition at 397 nm. A second laser beam at 866 nm is required to repump population from the $3d\ ^2D_{3/2}$ level to close the laser cooling cycle. The wavy line indicates spontaneous emission back to the ground state which is used for imaging the laser-cooled ions.

In the limit $|a_u|, q_u^2 \ll 1$, the trajectory of the ion is approximately given by [17]

$$u(t) \approx u_0 \cos(\omega_u t + \varphi)\left[1 + \frac{1}{2} q_u \cos(\Omega_{\mathrm{RF}} t)\right], \tag{3}$$

where φ is a phase determined by its initial position and velocity. The motion of the ion is periodic and separates into two components. The first term in Equation (3) corresponds to a slow 'secular' motion with frequencies

$$\omega_u = \frac{1}{2}\Omega_{\mathrm{RF}}\sqrt{a_u + \frac{1}{2}q_u^2} \tag{4}$$

and amplitudes $u_0 \equiv x_0, y_0, z_0$. Note that in the absence of additional static fields $\omega_x = \omega_y$. The second term is referred to as 'micromotion' and represents a fast oscillating motion superimposed on the secular motion which is constantly driven by the RF fields. If $|a_u|, q_u^2 \ll 1$, the two motions can be adiabatically separated [8,10,12,13,19]. In this limit, it can be shown that the secular motion in the radial (x, y) direction is governed by a time-independent pseudopotential which corresponds to the average kinetic energy stored in the micromotion and is approximately given by

$$\Phi^*(x, y) = \frac{1}{2} m\left(\omega_x^2 x^2 + \omega_y^2 y^2\right). \tag{5}$$

2.2. *Laser cooling of atomic ions*

Laser cooling [20] of the translational motion can be achieved in atomic ions with a simple energy-level structure which allows the implementation of closed optical cycles, for instance the alkaline-earth ions Be^+, Mg^+, Ca^+, Ba^+, and Sr^+. Laser cooling of trapped ions was first achieved by Wineland *et al.* [21] and Neuhauser *et al.* [22] and has since become a standard technique [9,10,13,15,20].

During laser cooling, the kinetic energy of the ions is decreased by the transfer of momentum from the repeated absorption of photons from a laser beam. The cooling of the ion motion is achieved by slightly detuning the laser frequency to the red side of an atomic resonance (see Figure 1(b)). In this way, photons are preferentially absorbed by atoms moving antiparallel to the laser beam for which the frequency mismatch is compensated by the Doppler shift (Doppler laser cooling). The resulting momentum transfer slows the ions down. The excited atoms subsequently decay by spontaneous emission of photons in a pattern always having inversion symmetry. Over repeated absorption and emission cycles, the momentum transferred to the atoms by spontaneous emission (photon recoil) is thus averaged out, resulting in a net cooling effect from photon absorption from the laser beam. The limiting temperature T_{D} which can be achieved by this scheme is given by [20,23]

$$T_{\mathrm{D}} \approx \frac{\hbar\gamma}{2k_{\mathrm{B}}}, \tag{6}$$

where γ is the natural linewidth of the cooling transition. For typical ions used, T_{D} is on the order of 1 mK, e.g., $T_{\mathrm{D}} = 0.5\,\mathrm{mK}$ for the 397 nm cooling transition of Ca^+ shown in Figure 1(b). In contrast to neutral atoms [20], it is often sufficient to use a minimum of one

laser beam to cool the motion of the ions in all three spatial dimensions because anharmonicities of the trapping potential and/or the Coulomb interaction between ions couple all translational degrees of freedom.[2]

Because the pseudopotential in a linear Paul trap is approximately harmonic, the secular motion of an ion can be described as an harmonic oscillator. In the quantum limit, the motion is described by a series of discrete motional states $|n_u\rangle_m$ with motional quantum numbers $n_u = 0, 1, 2, 3, \ldots$ and energies $E_{n_u} = (n_u + 1/2)\hbar\omega_u, u \in \{x, y, z\}$ [10,13,15,24]. In the Lamb–Dicke regime in which the extension of the ion wavefunction is much smaller than the wavelength of the radiation coupling to the ion, transitions between motional states appear as sidebands modulated onto the atomic spectrum. Transitions of the form $|n_u\rangle_m \rightarrow |n_u - 1\rangle_m$ are termed red-sideband (RSB) transitions. The repeated excitation of RSB transitions can be used to reduce the kinetic energy of the ion and cool the ion down to the motional ground state of the ion trap $|n_u = 0\rangle_m$ [15,25]. The zero-point energy E_0 associated with the three-dimensional motional ground state $|n_x = 0,\ n_y = 0,\ n_z = 0\rangle$ represents the physical limit for the cooling of trapped ions. For secular trapping frequencies of 1 MHz, one finds $E_0/k_B = 11\,\mu K$.

2.3. *Coulomb crystals*

Upon laser cooling, the ions form Coulomb crystals in the trap. Coulomb crystallisation sets in when the potential energy E_{pot} between the ions exceeds their kinetic energy E_{kin}. More specifically, theoretical simulations have shown that a phase transition to a crystalline state occurs if the plasma-coupling parameter Γ defined by

$$\Gamma = \frac{E_{pot}}{E_{kin}} = \frac{Q^2}{4\pi\varepsilon_0 a_{WS} k_B T} \tag{7}$$

exceeds a value of $\Gamma \approx 150$ [26–28]. In Equation (7), the Wigner–Seitz radius $a_{WS} = (3/(4\pi\rho))^{1/3}$ represents the average distance between the ions where ρ is the ion density. Depending on the number of trapped ions and the trapping conditions, single localised ions, strings of ions or three-dimensional spheroidal structures are obtained [2,29,30]. The properties of Coulomb crystals can be studied experimentally by imaging the fluorescence of the ions generated during laser cooling as shown in Figure 2(a). Careful analysis of the images, for instance with the help of molecular-dynamics (MD) simulations, enables the determination of the number of ions in the crystal and the ion kinetic energies [2,3,30,31].

Motions of small amplitude of the Coulomb-crystallised ions can be described in terms of normal modes [32–34], in analogy to the small-amplitude vibrations of the atomic nuclei in a molecule. For large spheroidal crystals, many of the normal modes are surprisingly well described by modes of a cold uniformly charged liquid [35–38]. In general, laser cooling acts on the secular motion of the ions and by reducing its amplitude u_0, it also reduces the amplitude of the micromotion (see Equation (3)). The micromotion, however, is never completely cooled as it is constantly driven by the RF fields. It is only suppressed completely for ions located on the central trap axis where the RF fields vanish. The energy stored in the micromotion scales quadratically with the distance of the ion from the central trap axis, see Equation (5). Three-dimensional Coulomb crystals in which a large number of ions are situated off axis generally exhibit broad distributions of ion energies which

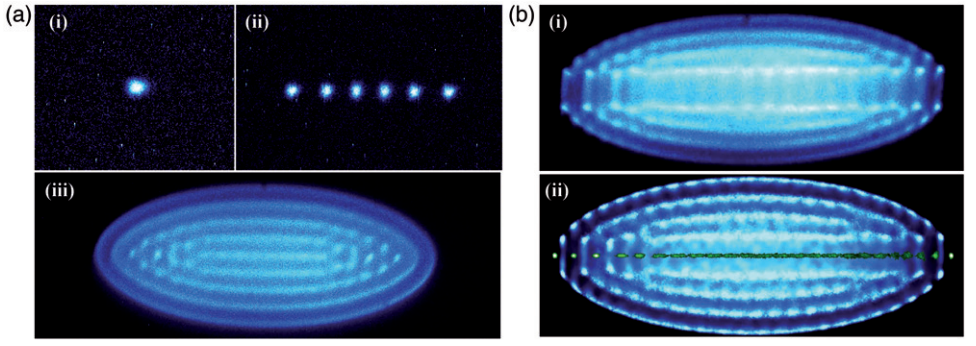

Figure 2. (Colour online) False-colour fluorescence images of laser-cooled Ca^+ ions in a linear Paul trap. (a) (i) A single laser-cooled ion, (ii) a string of six ions, (iii) a large spheroidal Coulomb crystal (not to scale with the images shown in (i) and (ii)). (b) (i) Bicomponent Coulomb crystal consisting of 925 laser-cooled Ca^+ ions and 24 sympathetically cooled N_2^+ ions. The molecular ions form a non-fluorescing region in the centre of the crystal. (ii) Molecular-dynamics simulation of the image in (i). The distribution of molecular ions in the crystal has been made visible in green in the simulation.

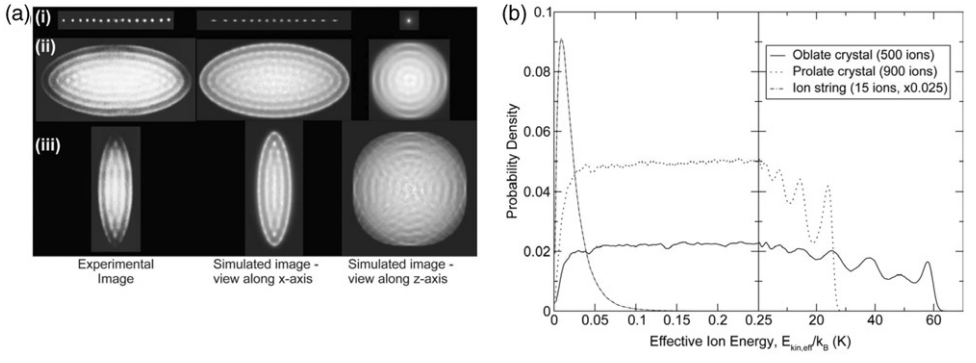

Figure 3. (a) Experimental and simulated Coulomb crystal images for (i) a string of 15 ions, (ii) a prolate crystal of 900 ions (long axis of spheroid along the trap axis), and (iii) an oblate crystal of 500 ions (long axis perpendicular to the trap axis). (b) Ion kinetic-energy distributions for the crystals in (a) obtained from the molecular-dynamics simulations including both secular and micromotion. From Ref. [30], reproduced by permission of The Royal Society of Chemistry.

depend on the number of ions and the shape of the crystals, see Figure 3. As can be seen from Figure 3, the kinetic-energy distributions are irregular so that it is not possible to assign a temperature to the ions. However, it can be shown that the secular kinetic energies associated with the motion in the pseudopotential (5) obey a Maxwell–Boltzmann distribution which allows to define a secular temperature T_{sec} for the ions [39].

2.4. *Sympathetic cooling of molecular ions*

The complexity of the molecular energy level structure usually prevents the implementation of closed optical cycles so that laser cooling is generally not applicable to molecules. The exception to this rule are molecules with nearly diagonal Franck–Condon factors in

which quasi-closed optical cycles can be realised, as has recently been demonstrated for SrF [40,41]. Direct laser cooling of trapped molecular ions has not been demonstrated so far, but theoretical studies have recently identified promising candidates for such experiments (BH^+, AlH^+) [42].

However, as these approaches are only applicable to a very limited set of molecular ions, alternative methods have to be employed. Over the past 15 years, sympathetic cooling [43,44] has emerged as a versatile method for cooling a broad range of molecular ions to millikelvin secular temperatures [1–3,45,46]. Sympathetic cooling relies on the simultaneous trapping of molecular ions with laser-cooled atomic ions. The ions exchange kinetic energy by elastic collisions which is removed by laser cooling on the atomic species. Thus, the atomic ions act as a coolant for the molecular ions resulting in the formation of bicomponent (or molecular) Coulomb crystals, see Figure 2(b). Sympathetic cooling of molecular ions down to temperatures in the range 7–70 K was first reported by Baba and Waki in 1996 [45]. However, sympathetic cooling of molecular ions to millikelvin secular temperatures leading to their Coulomb crystallisation was only achieved in 2000 by Mølhave and Drewsen [46]. Sympathetic cooling has since become the 'work-horse' technique in the field, and forms the basis of many experiments discussed in the present article.

Sympathetic cooling is applicable to a variety of species ranging from atomic ions [44,47,48], diatomic and small polyatomic ions [30,46,49–51] to large organic and biomolecular ions [52–55]. Because the strength of the pseudopotential depends on the mass of the ions (as can easily be seen by inserting Equations (2) and (4) into Equation (5)), sympathetically-cooled ions lighter than the coolant ions localise along and around the central axis of the trap, see the example of the Ca^+-N_2^+ bicomponent crystal shown in Figure 2(b). On the other hand, heavier sympathetically-cooled ions crystallise in shells around a central core of lighter laser-cooled ions. The dynamics of sympathetic cooling and the structure of bi- and multicomponent Coulomb crystals have been studied extensively using theoretical methods, see, e.g., Refs. [3,30,31,56–61]. In general, the efficiency of sympathetic cooling is optimal if the two ion species have similar mass-to-charge ratios m/z, in which case secular temperatures $T_{sec} \lesssim 10$ mK can be achieved [3,51]. However, even in extreme cases such as the sympathetic cooling of multiply-charged cytochrome c ions ($m/z \approx 729$ amu/e) with $^{138}Ba^+$, secular temperatures as low as 750 mK have been obtained [54].

2.5. *Coulomb crystals in alternative types of RF traps*

2.5.1. *RF multipoles*

Linear multipole traps consist of $2n$ ($n = 2, 3, 4, \ldots$) cylindrical electrodes evenly distributed around a circle. Compared to linear quadrupoles ($n = 2$) which represent the most commonly used variant, higher-order linear multipoles exhibit a flatter pseudopotential near the trap centre and steeper potential walls closer to the electrodes [8], see Figure 4(a). Ensembles of laser-cooled ions in octupole ($n = 4$) traps have recently been studied theoretically using MD simulations [62–65]. Coulomb crystals in these traps have been predicted to exhibit cylindrical shapes in contrast to the ellipsoidal structures observed in linear quadrupoles [62,64], see Figure 4(b). The cylindrical arrangement of the ions results from the superposition of a static endcap potential Φ_{END} which confines the ions along the

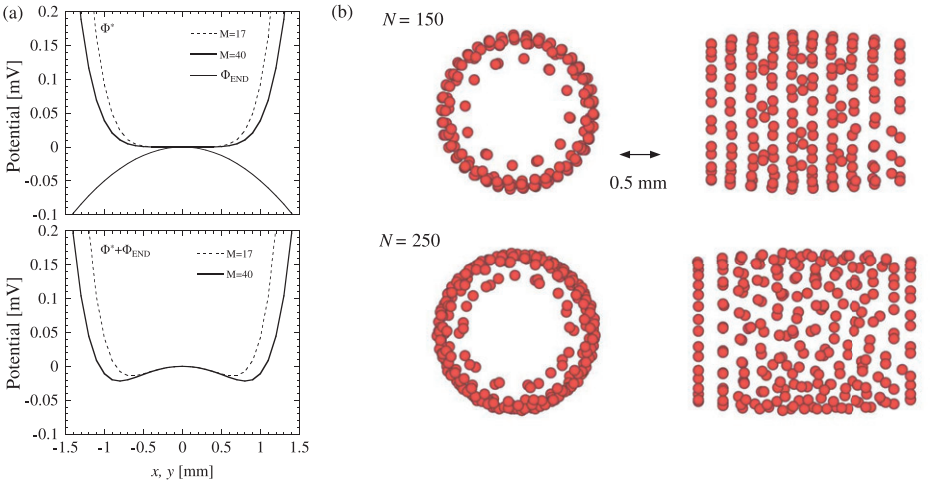

Figure 4. (Colour online) (a) Top panel: one-dimensional cuts through the pseudopotential Φ^* for ions with masses $M = 17$ and 50 and the static endcap potential Φ_{END} along the radial (x, y) directions of a linear octupole trap. Bottom panel: superposition $\Phi^* + \Phi_{END}$ illustrating the generation of a saddle point at the trap centre $x = y = 0$ and the formation of potential minima off axis. (b) Molecular-dynamics simulations of cylindrical Coulomb crystals with $N = 150$ and 250 Ca^+ ions in an octupole trap. From Ref. [62], copyright (2007) by the American Physical Society.

multipole axis, but is repulsive in the radial (x, y) direction, with the radial pseudopotential Φ^*. Because close to the trap axis the static potential is more strongly curved than the pseudopotential ($\Phi_{END} \propto -r^2$ compared to $\Phi^* \propto +r^6$ [8]), the total potential exhibits a saddle point at $r = 0$, see Figure 4(a). The minimum of the potential around which the cold ions localise assumes the shape of a cylinder centred on the axis [62,64]. Experimental evidence for such cylindrical ion ensembles has been observed recently [66], however, further studies are clearly desirable to explore in more detail the properties of these unusual Coulomb crystals.

2.5.2. *Microstructured traps on chips*

Recently, microstructured RF devices on chips have been developed as new trapping architectures for experiments with laser-cooled ions, notably in the context of quantum information processing [68–71]. Microstructured traps are more challenging to manufacture and operate and often exhibit reduced trap depths in comparison to conventional linear Paul traps. On the other hand, they enable the implementation of large interlinked trapping networks which offer more flexibility for manipulating the ions.

Surface-electrode traps are a variant of microtraps in which all electrodes are arranged in a plane. A widely used design consists of a 'five-wire' geometry which is formed by projecting the electrodes of a linear Paul trap onto a surface [72], see Figure 5(a). As a result, the quadrupolar symmetry of the potential is broken and the pseudopotential exhibits a saddle point above the surface through which the ions can escape (Figure 5(b)). The potential difference between the saddle point and the trap minimum defines the trap depth which is typically on the order of a few hundred meV. This can be compared with

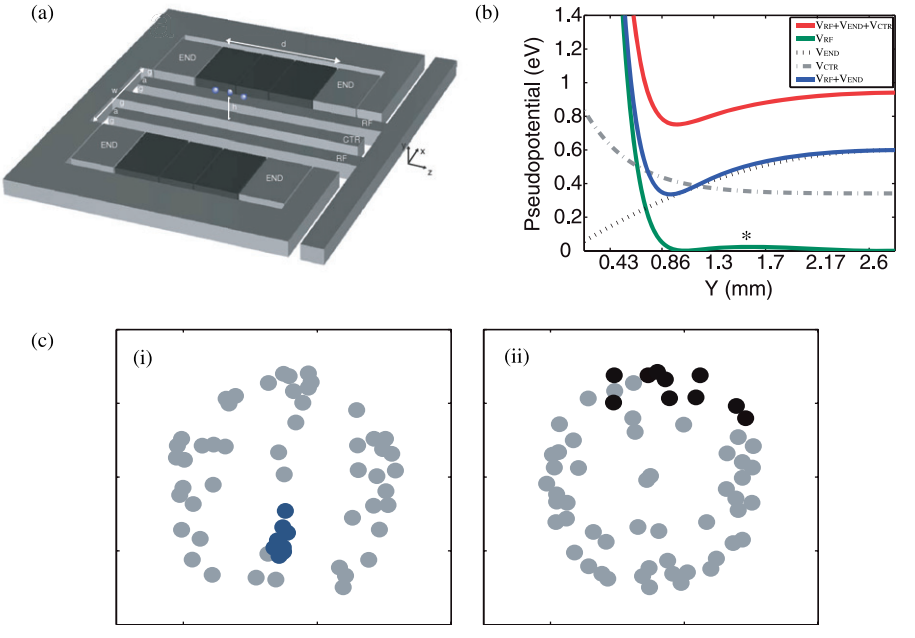

Figure 5. (Colour online) (a) Schematic of a 'five-wire' surface electrode (SE) ion trap exhibiting two radio-frequency (RF), four endcap (END) and one central (CTR) electrode. (b) Cut through the trap potential in the *y* direction (perpendicular to the surface) at the trap centre. The RF pseudopotential (green line) exhibits a saddle point (indicated by the asterisk) over which ions can escape. The trap depth in the *y* direction (defined as the potential difference between the saddle point and the minimum) is considerably increased upon the application of a static endcap voltage (blue line). (c) Molecular-dynamics simulations of the structures of bicomponent Coulomb clusters in a SE trap. (i) 10 N_2^+ ions (blue dots) and (ii) 10 CaH^+ ions (black dots) in Coulomb clusters of 50 laser-cooled Ca^+ ions (light grey dots). The asymmetric distribution of the ions results from the asymmetries of the trap potential shown in (b). From Ref. [67], reproduced by permission of the PCCP Owner Societies.

depths up to several eV achieved in typical linear Paul traps. Although surface-electrode traps are now widely used in atomic-ion experiments, see, e.g., Refs. [70,71] and references therein, the sympathetic cooling of molecular ions in these type of traps has not been reported so far. Georgescu *et al*. have recently performed a theoretical characterisation of the properties of bicomponent ion clusters in a five-wire surface electrode trap [67]. It was found that large multicomponent ion clusters can exhibit distinctly asymmetric ion configurations as a result of the asymmetric trap potential. The ion species in a bicomponent cluster were also predicted to segregate asymmetrically, see Figure 5(c). The spatial distributions of the ions and their energies are also strongly affected by the endcap and other static fields which push the ions away from the RF null line, the central trap axis on which the RF fields vanish.

3. State preparation of sympathetically cooled molecular ions

Sympathetic cooling is mediated by collisions between atomic and molecular ions which are dominated the long-range Coulomb repulsion. Consequently, the effective interaction

is nearly isotropic. The very small residual anisotropy will in principle lead to a coupling of the internal molecular degrees of freedom to the translational motion of the ions. However, since the quantised frequencies of the rovibrational transitions of the molecular ions are many orders of magnitude higher than the typical normal mode frequencies of the Coulomb crystals, this coupling is non-resonant and very weak. As a consequence, the vibrational and in particular the rotational motion are not cooled and ensembles of translationally cold, but internally warm molecular ions are obtained. Owing to the long trapping time in typical experiments (>minutes), the internal-state populations are usually in thermal equilibrium with the ambient room-temperature black-body-radiation field [73–75]. This situation stands in contrast to cooling with a cryogenic buffer gas which affects both the internal and translational degrees of freedom [8,76,77]. However, in buffer-gas-cooling experiments the lowest temperatures are limited to several kelvins, and Coulomb crystals are generally not obtained.

The preparation and control of the internal quantum state of sympathetically cooled molecular ions is a necessary prerequisite for a number of applications, ranging from state-controlled collision studies over precision spectroscopy of single ions to possible applications in quantum-information processing. This problem was already recognised in the early days of sympathetic-cooling experiments when Drewsen and coworkers proposed several schemes for the state-preparation of sympathetically cooled molecular ions [78–81]. Recently, two different experimental approaches have been implemented to overcome this problem.

3.1. *Optical pumping*

Based on the proposal by Vogelius *et al*. [78], Staanum *et al*. [82] and Schneider *et al*. [83] recently implemented 'rotational laser cooling' schemes to achieve the accumulation of population in the rotational ground state of sympathetically cooled MgH^+ and HD^+ ions. Their approach relies on the optical pumping of the population from rotational levels of the vibrational ground state to vibrationally excited states. The relevant rovibrational transitions are carefully chosen so that subsequent spontaneous emission back to the vibrational ground state populates the rotational ground state owing to selection rules.

In the experiments on MgH^+ [82], the population was continuously pumped from the $v''=0$, $N''=2$ level to the $v'=1$, $N'=1$ level using a continuous-wave infrared laser, see Figure 6(a)(i). Here, N and v denote the rotational and vibrational quantum numbers and $''$ and $'$ stand for the lower and upper state of the infrared transition, respectively. Because of the rotational selection rule $\Delta N = N' - N'' = \pm 1$, spontaneous emission from the excited rovibrational state leads to the accumulation of population in the $N''=0$ and 2 levels. Ambient black-body radiation induces a redistribution of the population among the rotational levels, including $N''=2$ from where it is immediately re-pumped to the $v'=1$ state. Overall, this scheme results in an accumulation of population in the $N''=0$ level after several tens of seconds. In this way, steady-state populations of 37% in the $N''=0$ state were achieved which corresponds to an almost 15-fold increase in comparison to the population in thermal equilibrium at room temperature, see Figure 6(b).

The efficiency of the population-accumulation scheme can further be increased by using additional pumping lasers, as demonstrated in the experiments on HD^+ [83]. By employing two IR laser beams resonant with the $(v''=0,\ N''=1) \rightarrow (v'=2,\ N'=0)$ and

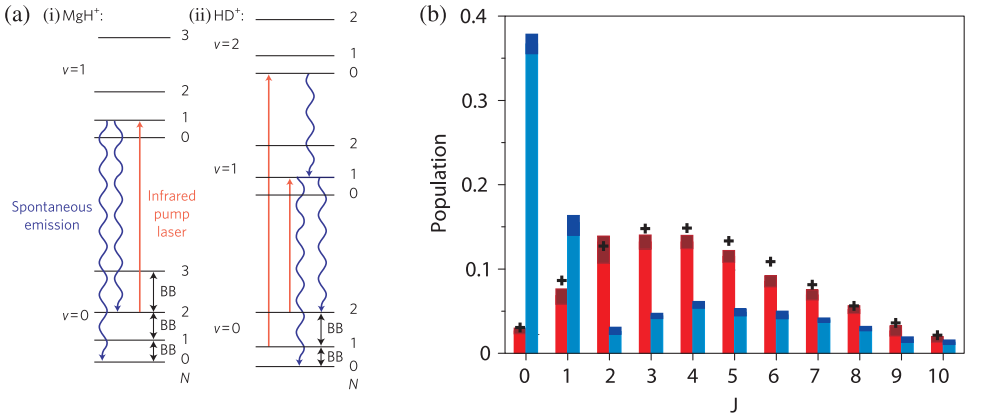

Figure 6. (Colour online) (a) Rotational laser-cooling schemes for accumulation of population in the rotational ground state $N=0$ in (i) MgH^+ [82] and (ii) HD^+ [83]. BB stands for the radiative coupling between rotational levels by black-body radiation. (b) Distribution of the population over rotational levels $J \equiv N$ in MgH^+ before (red bars) and after (blue bars) rotational laser cooling. Adapted by permission from Macmillan Publishers Ltd: Nature Physics [82,84], copyright (2010).

$(v''=0,\ N''=2) \rightarrow (v'=1,\ N'=1)$ transitions, see Figure 6(a)(ii), the efficiency of the population transfer into the $v''=0$, $N''=0$ state could be increased to reach populations up to 78%.

3.2. *State-selective generation of molecular ions*

An alternative method for the generation of state-selected, sympathetically cooled molecular ions has recently been demonstrated by Tong *et al.* [51,75]. In these experiments, N_2^+ ions were produced in a well-defined rotational level using threshold-photoionisation, followed by the sympathetic cooling of their translational motion. The technique relies on the fact that photoionisation is subject to optical selection and propensity rules which lead to the generation of only a limited number of rotational states when a molecule is ionised out of a well-defined initial state [85]. By setting the photoionisation energy slightly above the lowest ionic state accessible by the selection rules (threshold ionisation), molecular ions could be generated in a single rotational level.

N_2 molecules were ionised from a collimated supersonic gas expansion passing close to the centre of the ion trap. In an initial two-photon excitation step, well-defined rotational levels J' of the $a''\,^1\Sigma_g^+$ excited electronic state of N_2 were populated (e.g., $J'=2$ as indicated in Figure 7(a)). Photoionising transitions out of the a'' electronic state of N_2 are subject to the rotational propensity rule $\Delta N = J' - N^+ = 0, \pm 2$ [86]. Here, J' and N^+ denote the rotational quantum numbers in the intermediate and cationic state, respectively. By setting the ionisation energy slightly above the $N^+=0$ ionisation threshold, N_2^+ ions were only produced in the rotational ground state.

After sympathetic cooling, the rotational-state populations were probed using laser-induced charge-transfer (LICT) spectroscopy [51,75]. This method relies on the fact that N_2^+ ions can undergo charge transfer with Ar atoms only in vibrationally excited states,

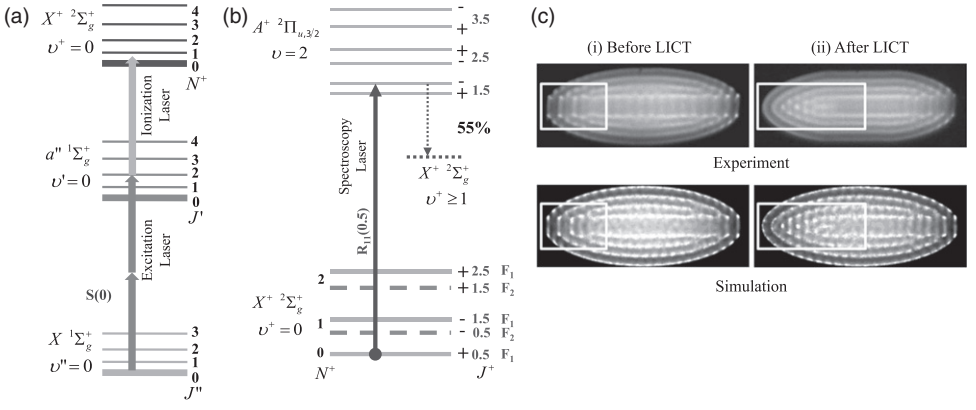

Figure 7. (a) [2 + 1′] resonance-enhanced threshold-photoionisation sequence for the selective generation of N_2^+ ions in the rotational ground state $N^+ = 0$ from Ref. [51]. (b) The population in the $N^+ = 0$ level was probed by a laser-induced charge transfer (LICT) scheme which was initiated by optical pumping into vibrationally excited states. The efficiency of this population transfer amounted to 55%. The vibrationally excited N_2^+ ions underwent charge-transfer reactions with Ar atoms and the fraction of reacted molecular ions was taken as a measure of the initial rotational level population in $N^+ = 0$. (c) Fluorescence images of a Ca^+/N_2^+ bicomponent Coulomb crystal obtained (i) after state-selective generation of N_2^+ ions using the scheme in (a) and sympathetic cooling, (ii) after LICT. By comparison with the simulated images, it was inferred that 51±6% of the N_2^+ ions underwent charge transfer, translating into a population of 93±11% in $N^+ = 0$. From Ref. [51], copyright (2010) by the American Physical Society.

but not in the vibrational ground state for energetic reasons [87]. For that purpose, the N_2^+ ions were excited out of the $v^+ = 0$, $N^+ = 0$ level to the $A\ ^2\Pi_{u,\,3/2}$ first excited electronic state, see Figure 7(b). Subsequent radiative decay led to the population of vibrationally excited levels of the electronic ground state with an efficiency of 55%. The vibrationally excited N_2^+ ions underwent charge-transfer reactions with Ar gas leaked into the chamber. From the fraction of destroyed N_2^+ molecules, the initial population in the $v^+ = 0$, $N^+ = 0$ level was inferred. Figure 7(c) shows a LICT measurement probing the population in the $N^+ = 0$ rotational level prepared by the threshold ionisation sequence shown in Figure 7(a). The population was found to be 93±11%, suggesting an efficiency close to unity in the initial state-preparation step.

3.3. *Comparison of state-preparation schemes*

Both approaches, optical pumping and threshold ionisation, have proved successful in the generation of sympathetically cooled molecular ions with a high degree of state purity. The optical pumping schemes employed in Refs. [82,83] provide continuous cooling of the rotational degrees of freedom using strong dipole-allowed IR transitions. Therefore, they are particularly suited for polar ions. However, they are not applicable to apolar species which do not exhibit a dipole-allowed IR spectrum. Threshold-photoionisation on the other hand, while being equally applicable to polar and apolar species, is particularly attractive for apolar ions which do not couple to the ambient black-body radiation field

and therefore allow the preservation of the originally prepared state over extended periods of time.

Very recently, a number of alternative optical-pumping schemes for internal-state preparation have been proposed. These approaches rely on the coupling of the internal state with the motional state of the ions using Raman transitions in the resolved-sideband regime [88–90]. At the expense of additional experimental overhead, these methods are potentially applicable to both polar and apolar species, and are predicted to be faster than black-body-radiation assisted optical-pumping schemes [88]. However, as individual motional sidebands need to be addressed, they will effectively be restricted to very small ensembles of sympathetically cooled molecular ions.

4. Chemistry with cold ions

Studies of chemical reactions under extreme conditions represent one of the key applications of Coulomb-crystallised ions. Early investigations focused on reactions of large Coulomb-crystallised ensembles of laser- or sympathetically cooled ions with various gases leaked into the vacuum chamber, e.g., $Mg^+ + H_2$ [46], $H_3O^+ + NH_3$ [91], $Ca^+ + O_2$ and CO [29], $Be^+ + H_2$ and $H_3^+ + O_2$ [49], Ar^+, N_2^+ and $H_2^+ + H_2$ [50]. More recently, however, the intriguing properties of Coulomb-crystallised ions have allowed to push chemical studies towards two extremes which have not been accessible before: single-ion experiments and ultralow-energy ion-neutral reaction studies.

4.1. *Chemical reactions with single ions*

In a pioneering study, Drewsen and coworkers [92] reacted one ion in a Coulomb crystal consisting of two laser-cooled Ca^+ ions with oxygen gas to form a CaO^+ molecular ion which was sympathetically cooled by the remaining atomic ion. The mass m of the molecular ion was subsequently determined using a resonant-excitation technique. A two-ion crystal exhibits two normal modes of the combined axial motion of the ions, a centre-of-mass mode and a breathing mode, which exhibit distinct motional frequencies [33,34]. Because the frequencies depend on the mass of the ions, their measurement was used as a means for the mass spectrometry of the constituents of the two-ion Coulomb crystal.

In Ref. [92], the centre-of-mass mode was resonantly excited by subjecting the ions to a periodic drive. This perturbation was generated either by applying an additional RF potential to the trap or by modulating the cooling-laser beam intensity. The resonant excitation of the ions manifested itself in the blurring of the ion images. Using phase-sensitive detection of the ion motion, the position of the resonance and hence the mass of the sympathetically cooled ion was determined with a resolution on the order of $m/\Delta m \approx 10^4$. A detailed characterisation of this method has recently been given in Ref. [93].

This study demonstrated both the possibility to observe chemical reactions with single ions and sympathetically cool the single product ions, and the capability to perform highly precise mass-spectrometric measurements on single ions. In subsequent experiments by the same group, these techniques were employed in the measurement of unusual isotopic branching ratios in the reaction of Mg^+ ions with HD molecules [94] and in the study of consecutive photodissociation events in single molecular ions [52].

4.2. *Cold chemistry*

The study of chemical reactions at ultralow collision energies $E_{\mathrm{coll}}/k_{\mathrm{B}} \ll 1$ K, often referred to as 'cold chemistry', has received considerable attention over the last few years [95–97]. The reasons for this interest lie in the intriguing features of reactive collisions at ultralow energies. In this regime, collisions are dominated by only a few (in the extreme case even only one) partial waves, allowing the study of quantum effects which depend on the collisional angular momentum, e.g., reactive scattering resonances and tunnelling through centrifugal barriers. The dynamics of ultralow-energy collisions is dominated by long-range interactions, enabling the detailed characterisation of the role of 'universal' chemical forces. Moreover, by accurately determining the collision energy and internal quantum state of the reaction partners and by the application of external electric and magnetic fields, prospects open up to study and control chemical processes at an unprecedented level of accuracy [98,99].

Most cold-chemistry studies thus far have focused on collisions and reactions between neutral molecules [95,99–104]. Ion-neutral reactions on the other hand represent an important class of processes exhibiting a different chemical behaviour [96,105–108]. Theoretical models at varying levels of sophistication have been developed to describe low-temperature ion-neutral reactions. These range from classical Langevin capture (see, e.g., Refs. [109,110] and references therein), and adiabatic capture [108,111], to close-coupled scattering equations and quantum-defect theory [106,107,112–114]. Capture models assume that ion-neutral collisions are barrierless processes dominated by the interaction between the charge and permanent or induced dipoles [107,108,111]. As a consequence, the reaction dynamics follow 'universal' behaviour whereby a chemical reaction is initiated by long-range attractive forces and subsequently occurs with unit probability at short range. In this context, it is particularly interesting to assess the validity of these models in the cold regime in which only few partial waves contribute to the collision and quantum effects become important.

In order to study cold collisions between ions and neutrals, both types of reaction partners need to be translationally cold. The generation of samples of cold neutral molecules has made impressive progress over the last decade. By now, an arsenal of different methods has become available, see, e.g., the comprehensive reviews [96,115,116] and the literature cited therein. Similarly to molecular ions, it is not only essential to cool the translational motion of the neutrals, but also to accurately control their internal, i.e., rotational, vibrational and hyperfine, quantum state [117–120].

In 2008, Willitsch *et al.* [105] combined an ion trap for the generation of Coulomb crystals with an electrostatic velocity selector for the generation of continuous beams of cold neutral molecules [121]. A schematic of the experimental setup is presented in Figure 8(a). The velocity selector consists of a bent electrostatic quadrupole to guide a thermal beam of polar molecules emitted from an effusive source. At the bend, the slowest molecules are forced around the corner, whereas fast molecules are lost from the guide. Subsequently, the slow molecules enter the ion trap located at the exit of the quadrupole. Here, collisions between laser- and sympathetically cooled ions and the velocity selected neutrals occur. Mechanistic information on the reactions studied were inferred from the comparison of experimental rate constants with theoretical predictions. The rate constants were obtained by analysing the rate of decrease of the reactant ions in terms of a pseudo-first-order kinetic model as illustrated in Figure 8(b) and discussed in detail in Ref. [105].

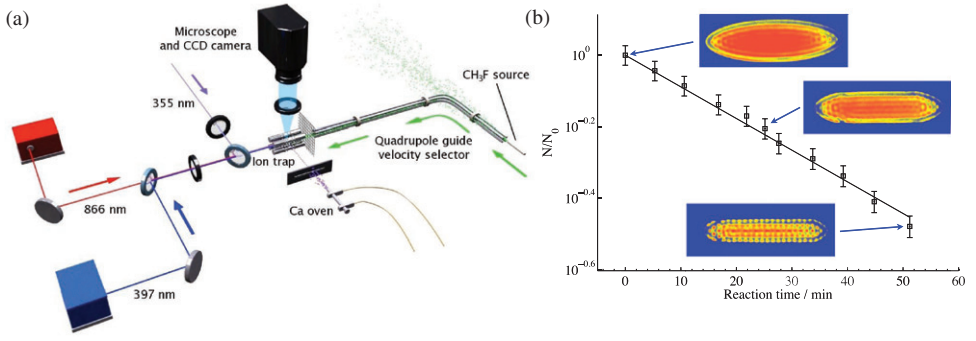

Figure 8. (a) Experimental setup for the study of cold ion-neutral reactive collisions by combining a Coulomb-crystal apparatus with an electrostatic velocity selector for polar neutral molecules [105]. (b) Fraction of laser-cooled Ca^+ ions remaining in the Coulomb crystal as a function of the time of reaction with velocity-selected CH_3F molecules. The solid line represents a fit to an integrated pseudo-first-order rate law from which bimolecular rate constants for the reaction $Ca^+ + CH_3F \rightarrow CaF^+ + CH_3$ were obtained [105]. Panel (a) from Ref. [105], copyright (2008) by the American Physical Society. Panel (b) from Ref. [2], reproduced by permission of the PCCP Owner Societies.

This approach was applied to the study of a range of reactions between laser- and sympathetically cooled ions and velocity-selected neutrals including $Ca^+ + CH_3F$ [30,105], $OCS^+ + ND_3$ [30], $Ca^+ + CH_2F_2$, and $Ca^+ + CH_3Cl$ [122] down to collision energies corresponding to a few kelvin. These experiments enabled the characterisation of dynamical effects in cold ion-molecule reactions such as the role of low-lying potential barriers and electronic excitation of the reactants [30,122].

4.3. *Ion-atom hybrid traps*

Recently, several groups have combined ion traps with traps for ultracold atoms which enabled them for the first time to enter the millikelvin regime in ion-neutral collision experiments. Besides opening up prospects for the study of ion-neutral collisional processes at extremely low temperatures, such ion-atom 'hybrid' traps also hold promise for the exploration of unusual mesoscopic quantum systems consisting of ions loosely bound to atoms in an ultracold gas [123] and the study of photo- and magnetoassociation processes in mixed ion-neutral systems [124–126]. Moreover, the gas of ultracold atoms could potentially be used to sympathetically cool the ions below the Doppler limit without the need for resolved-sideband-cooling schemes [127,128].

The properties of ensembles of simultaneously trapped ultracold ions and atoms and collisional processes occurring in them were first described theoretically by Côté and coworkers [112,123,129,130]. The first detailed proposal for an experimental implementation was based on the combination of a magneto-optical trap (MOT) for Na atoms with a linear Paul trap for laser-cooled Ca^+ ions [131]. The first experimental realisation of a hybrid trap was reported by Vuletić and coworkers who combined a Yb-MOT with a surface-electrode trap for laser-cooled Yb^+ ions [132,133]. Following these pioneering

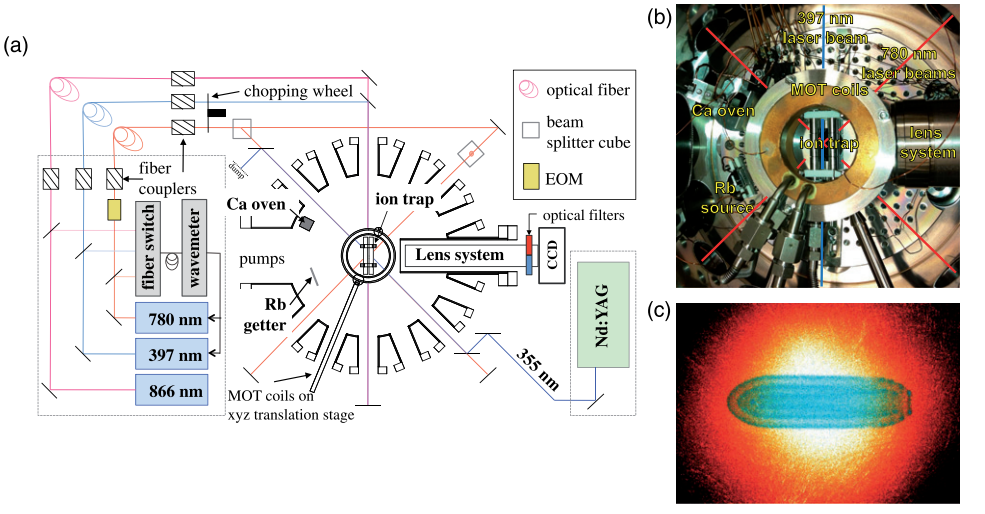

Figure 9. Hybrid traps. (a) Experimental setup from Ref. [136] for the combination of a linear Paul trap for laser-cooled Ca^+ ions and a vapour-cell magneto-optical trap (MOT) for ultracold Rb atoms. (b) Close-up photograph of the ion and magneto-optical traps. (c) False-colour fluorescence images of a Coulomb crystal of laser-cooled Ca^+ ions (blue) in a cloud of ultracold Rb atoms. Panels (a) and (c) from Ref. [136], copyright (2011) by the American Physical Society.

studies, several groups have developed similar experiments by combining ion traps with either MOTs [134–136] or trapped Bose–Einstein condensates [125,128].

As an example, Figures 9(a) and (b) show the hybrid-trap setup described in Ref. [136]. A linear Paul trap for the laser- and sympathetic cooling of ions has been combined with a vapour-cell MOT for ultracold Rb atoms. The MOT [137] consists of a pair of coils in anti-Helmholtz configuration which generate a quadrupolar magnetic field with a gradient of ≈ 20 G/cm in the centre. Rb atoms are captured and laser-cooled from ambient vapour by three pairs of 780 nm-diode-laser beams counterpropagating along the x, y and z axes. Optical forces generated by transitions between Zeeman levels in the inhomogeneous magnetic field trap the atoms in the centre. With this setup, typically 10^5–10^6 atoms at densities of $10^9\,\mathrm{cm}^{-3}$ are trapped and temperatures in the range of 150–200 μK are achieved. Ca^+ ions are laser cooled in the ion trap using standard procedures as outlined in Section 2.2. A typical experiment is illustrated in Figure 9(c) which shows a false-colour fluorescence image of a Ca^+ Coulomb crystal immersed in a cloud of ultracold Rb atoms.

Several experimental studies focused on the action of the ions on the cloud of ultracold atoms [125,128]. These studies also demonstrated the sympathetic cooling of the ions by the ultracold atoms down to temperatures comparable to Doppler-laser-cooling experiments [128]. Recently, chemical processes occurring in the different types of hybrid traps have shifted into the focus of attention. Whereas in collisions between isotopes of Yb and Yb^+ fast near-resonant charge exchange in accordance with Langevin theory was observed [133,138], only very slow reactive processes were found to occur in collisions between Rb and Yb^+ [124] and Rb and Ba^+ [125]. For Rb/Yb^+, the observations were rationalised in terms of slow non-adiabatic and radiative charge exchange [124]. In the latter study, it was

also speculated whether the formation of molecular ions is possible under the highly dilute and cold experimental conditions prevailing in hybrid traps, but no experimental evidence was found. Very recently, Rellergert *et al.* [135] observed very large reaction rates between cold Yb^+ ions and Ca atoms in a hybrid trap. In a recent study on the $Ca^+ + Rb$ system, Hall *et al.* [136] observed a significant increase of the reaction rates upon electronic excitation of the collision partners and the generation of molecular ions by radiative association.

Although these studies have so far been restricted to chemically 'simple' ion-atom collisions, they have already demonstrated the great potential of hybrid traps for collision and reaction studies. The chemistry observed in ion-atom hybrid traps owes itself to the capacity of ions to exchange charge through non-adiabatic and radiative processes as well as to form molecules by radiative association. In electronically excited collisions, these processes are usually feasible through a variety of channels resulting from the high density of states in ion-atom hybrid systems [136]. This situation stands in contrast to the comparatively smaller range of chemical processes which can occur in neutral atom traps [139].

Apart from chemical studies, future perspectives of hybrid traps lie in the refinement of the sympathetic cooling of ions with ultracold atoms to achieve ion temperatures in the sub-millikelvin regime. Besides providing a new cooling method potentially rivalling resolved-sideband cooling, this development would also constitute an important step towards exploring new unusual mesoscopic quantum systems predicted by theory [123].

5. Precision spectroscopy

Precision spectroscopy, i.e., spectroscopic experiments at an extremely high resolution, on cold molecules and ions has recently received considerable interest as a means to explore fundamental physical concepts such as a potential time variation of fundamental constants [140–144], the dipole moment of the electron [145,146] and the energy difference between enantiomeric forms of chiral molecules [147]. Cold trapped ions exhibit a range of advantages for applications in this field. First, experiments on single trapped ions avoid inhomogeneous spectral line broadening resulting from ensemble averaging. Second, the low translational temperatures of the ions minimise Doppler line broadening. Third, the long storage times allow experiments over extended periods of time. Fourth, the ion trap in the UHV chamber constitutes a well-defined experimental environment in which interactions with the surroundings are minimised or well controlled. Therefore, it is not surprising that trapped atomic ions currently represent the most advanced systems for precision frequency measurements [141].

5.1. *Resonance-enhanced multiphoton dissociation spectroscopy*

Pioneering experiments towards precision measurements on sympathetically cooled molecular ions were performed by Schiller and coworkers [148,149]. These results were recently reviewed in Ref. [3] and are briefly mentioned here for completeness.

In these experiments, high-resolution infrared spectroscopy on sympathetically cooled HD^+ ions was performed. The rovibrational transitions $(v'' = 0,\ N'' = 2) \rightarrow (4,\ 1)$ and $(0,\ 2) \rightarrow (4,\ 3)$ at a wavelength around 1.4 μm were studied in samples of about 40–100

molecular ions sympathetically cooled into a Be^+ Coulomb crystal. Spectroscopic transitions were detected using a resonance-enhanced multiphoton dissociation (REMPD) scheme. The absorption of an additional 266 nm photon from the vibrationally excited state resulted in the photofragmentation of the ions. The photofragmentation rate was derived from time-resolved resonant-excitation mass spectrometric measurements as a measure of the IR absorption strength. At a resolution of ≈40 MHz limited by the residual micromotion-induced Doppler shift, the spectral line positions could be determined with an absolute accuracy of 450 kHz [74].

In analogy to previous experiments on atomic ions [141,150], further progress towards precision measurements on molecular ions could be achieved by performing spectroscopic experiments on single particles. This would allow to remove the effects of ensemble averaging and also to avoid micromotion-induced Doppler broadening by localising the ion on the RF null line in the trap. In addition, such experiments should ideally use a non-destructive spectroscopic technique to avoid variations in the experimental conditions resulting from repeated trap loading.

This approach would not only require extreme sensitivity allowing the detection of a spectroscopic transition in a single molecule trapped in ultrahigh vacuum, but would also necessitate the re-initialisation of the molecule in the relevant quantum state after every excitation cycle. For atomic systems, well-established methods to fulfil these requirements exist. For instance, efficient detection can be achieved by using an optical cycling transition, typically the one which is also used for Doppler laser cooling [150]. This scheme is ubiquitously used, e.g., to read out quantum registers in ion trap quantum-information processing [151]. However, such an approach is generally not applicable to molecules because of the lack of closed transitions.

5.2. *Quantum-logic spectroscopy*

A potential solution to this problem is 'quantum logic spectroscopy'. This scheme was originally demonstrated in a two-ion system consisting of a laser-cooled Be^+ ion and a sympathetically cooled Al^+ ion [152]. The principle of quantum-logic spectroscopy relies on the entanglement of the spectroscopy ion S (Al^+) with the 'logic ion' L (Be^+). For this purpose, a quantum gate is implemented which maps the state of S onto L from which it is read out via an optical cycling transition.

The quantum gate implemented in Ref. [152] for detecting the Al^+ 'clock' transition ($^1S_0$, $F=5/2 \rightarrow {}^3P_1$, $F'=7/2$), denoted ($|\downarrow\rangle_S \rightarrow |\uparrow\rangle_S$), requires an auxiliary Raman transition between the ($F=2$, $m_F=-2) \equiv |\downarrow\rangle_L$ and ($F'=1, m'_F=-1) \equiv |\uparrow\rangle_L$ levels in the Be^+ $^2S_{1/2}$ ground state, see Figure 10(a). Here, F and m_F denote the total angular momentum and its associated magnetic quantum numbers and $'$ refers to the relevant excited states $|\uparrow\rangle$. The operation of the gate is illustrated in Figure 10(b). In the first step, both ions are prepared in the states $|\downarrow\rangle_S$ and $|\downarrow\rangle_L$. Additionally, the two-ion string is initialised in the motional ground state $|0\rangle_m$ of the combined centre-of-mass motion by resolved-sideband cooling, resulting in the overall state $\Psi_0 = |\downarrow\rangle_S|\downarrow\rangle_L|0\rangle_m$ (Figure 10(b) A). By exciting the spectroscopy ion close to resonance, Rabi flopping between $\downarrow\rangle_S$ and $|\uparrow\rangle_S$ is induced creating a coherent superposition between the two states (Figure 10(b) B):

$$\Psi_0 \rightarrow \Psi_1 = \left(\alpha|\downarrow\rangle_S + \beta|\uparrow\rangle_S\right)|\downarrow\rangle_L|0\rangle_m, \tag{8}$$

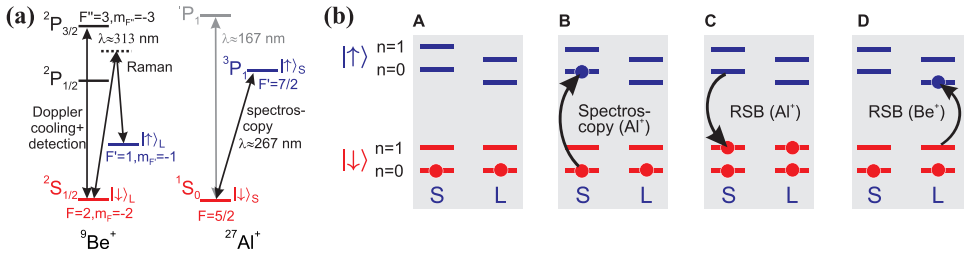

Figure 10. Quantum-logic spectroscopy of a single sympathetically cooled Al^+ ion [152]. (a) Energy-level schemes and relevant transitions in the 'logic ion' L ($^9Be^+$) and the 'spectroscopy ion' S ($^{27}Al^+$). (b) Quantum gate for detecting a spectroscopic transition in S by readout on L, see text for details. From Ref. [152], reprinted with permission from AAAS.

where $|\alpha|^2 + |\beta|^2 = 1$. A red-sideband π pulse (Figure 10(b) C) maps the spectroscopy ion's internal state onto the centre-of-mass mode

$$\Psi_1 \rightarrow \Psi_2 = |\downarrow\rangle_S|\downarrow\rangle_L\big(\alpha|0\rangle_m + \beta|1\rangle_m\big), \tag{9}$$

creating a superposition between the motional states $|0\rangle_m$ and $|1\rangle_m$. A final red-sideband π pulse on the logic ion (Figure 10(b) D) yields

$$\Psi_2 \rightarrow \Psi_3 = |\downarrow\rangle_S\big(\alpha|\downarrow\rangle_L + \beta|\uparrow\rangle_L\big)|0\rangle_m, \tag{10}$$

completing the transfer of the state of the spectroscopy ion onto the logic ion. The logic ion is then measured by projecting the state Ψ_3 onto $|\downarrow\rangle_L$ or $|\uparrow\rangle_L$ which can efficiently be distinguished by scattering photons via the optical cycling transition in the logic ion (see Figure 10a). By repeated execution of this scheme, the resonance frequency of the transition $|\downarrow\rangle_S \rightarrow |\uparrow\rangle_S$ is obtained by determining the probabilities $|\alpha|^2$ and $|\beta|^2$ as a function of the spectroscopy laser frequency.

Although technically rather involved, quantum-logic spectroscopy has been demonstrated to be a very powerful method for the precision spectroscopy of single atomic ions and now forms the basis of the Al^+ optical clock at NIST [141]. Various variations of this method aiming at the spectroscopy of single molecular ions have recently been put forward. These include straightforward adaptations of the scheme used for atomic ions [153], the use of Raman transitions and fs-laser frequency combs to drive sideband transitions for state preparation and detection in a two-ion crystal [89,90] and the implementation of state-dependent forces to either heat the crystal [74] or drive a geometric-phase gate [154]. Experiments in this direction are currently being pursued by several research groups.

6. Conclusions

The past few years have seen impressive progress in the field of sympathetically cooled molecular ions. New experimental methods have been developed which allow the control of their internal quantum state, chemical processes have been studied at the single-ion level, millikelvin temperatures have been reached in ion-atom collision experiments and spectroscopic measurements have been performed with high precision.

These recent developments have opened up a variety of perspectives for further progress. Based on the recently established techniques to prepare the internal quantum state of sympathetically cooled molecular ions, precision spectroscopic experiments on single molecules have now moved closer within reach. In the foreseeable future, these experiments will have a strong connection with developments in quantum information science, and indeed molecular ions might also emerge as a system for new applications in this context. Ion-neutral collision and reaction experiments will benefit from the improved capabilities to control both the internal quantum state of the ions and the collision energy. Finally, the intriguing possibilities of hybrid traps are just beginning to be explored. The current activity in the field is reflected by the increasing number of research groups working on topics related to sympathetically cooled molecular ions, laying the groundwork for future exciting discoveries and advances in this highly interdisciplinary field.

Acknowledgements

Financial support is acknowledged from the University of Basel, the COST Action 'Ion Traps for Tomorrow's Applications' and the Swiss National Science Foundation through the National Centre of Competence in Research 'Quantum Science and Technology' as well as grant nr. PP0022_118921.

Notes

1. Note that the q_u factor in Equation (2) differs by a factor of 2 from other sources in the literature because of a differing RF voltage configuration applied to the trap [13,18] or a different definition of the RF amplitude [11].
2. The need for only one cooling laser beam for trapped ions is actually also true for a perfect 3D harmonic potential provided the laser beam is not collinear with any main trap axis. This requirement can always be achieved as long as the trapping potential is not isotropic.

References

[1] M. Drewsen, I. Jensen, J. Lindballe, N. Nissen, R. Martinussen, A. Mortensen, P. Staanum, and D. Voigt, Int. J. Mass Spectrom. **229**, 83 (2003).
[2] S. Willitsch, M. T. Bell, A. D. Gingell, and T. P. Softley, Phys. Chem. Chem. Phys. **10**, 7200 (2008).
[3] B. Roth and S. Schiller, in *Cold Molecules*, edited by R. V. Krems, W. C. Stwalley, and B. Friedrich (CRC Press, Boca Raton, 2009), p. 651.
[4] W. M. Itano, J. J. Bollinger, J. N. Tan, B. Jelenković, X. P. Huang, and D. J. Wineland, Science **279**, 686 (1998).
[5] T. B. Mitchell, J. J. Bollinger, D. H. E. Dubin, X. P. Huang, W. M. Itano, and R. H. Baughman, Science **282**, 1290 (1998).
[6] K. Koo, J. Sudbery, D. M. Segal, and R. C. Thompson, Phys. Rev. A **69**, 043402 (2004).
[7] R. C. Thompson, S. Donnellan, D. R. Crick, and D. M. Segal, J. Phys. B **42**, 154003 (2009).
[8] D. Gerlich, Adv. Chem. Phys. **82**, 1 (1992).
[9] W. M. Itano, J. C. Bergquist, J. J. Bollinger, and D. J. Wineland, Phys. Script. **T59**, 106 (1995).
[10] P. K. Ghosh, *Ion Traps* (Clarendon Press, Oxford, 1995).
[11] M. Drewsen and A. Brøner, Phys. Rev. A **62**, 045401 (2000).
[12] R. E. March and J. F. Todd, *Quadrupole Ion Trap Mass Spectrometry*, 2nd ed (John Wiley & Sons, Hoboken, 2005).

[13] F. G. Major, V. N. Gheorghe, and G. Werth, *Charged Particle Traps* (Springer, Berlin, 2005).
[14] A. Drakoudis, M. Söllner, and G. Werth, Int. J. Mass Spectrom. **252**, 61 (2006).
[15] D. Leibfried, R. Blatt, C. Monroe, and D. Wineland, Rev. Mod. Phys. **75**, 281 (2003).
[16] J. D. Prestage, G. J. Dick, and L. Maleki, J. Appl. Phys. **66**, 1013 (1989).
[17] D. J. Berkeland, J. D. Miller, J. C. Bergquist, W. M. Itano, and D. J. Wineland, J. Appl. Phys. **83**, 5025 (1998).
[18] D. Wineland, in *Les Houches*, edited by D. Esteve, J. M. Raimond, and J. Dalibard (Elsevier, Amsterdam, 2004), Vol. 79, p. 261.
[19] H. G. Dehmelt, Adv. At. Mol. Phys. **3**, 53 (1967).
[20] H. J. Metcalf and P. van der Straten, *Laser Cooling and Trapping* (Springer, New York, 1999).
[21] D. J. Wineland, R. E. Drullinger, and F. L. Walls, Phys. Rev. Lett. **40**, 1639 (1978).
[22] W. Neuhauser, M. Hohenstatt, P. Toschek, and H. Dehmelt, Phys. Rev. Lett. **41**, 233 (1978).
[23] S. Stenholm, Rev. Mod. Phys. **58**, 699 (1986).
[24] D. J. Wineland, C. Monroe, W. M. Itano, D. Leibfried, B. E. King, and D. M. Meekhof, J. Res. Natl. Inst. Stan. **103**, 259 (1998).
[25] C. Monroe, D. M. Meekhof, B. E. King, S. R. Jefferts, W. M. Itano, D. J. Wineland, and P. Gould, Phys. Rev. Lett. **75**, 4011 (1995).
[26] E. L. Pollock and J. P. Hansen, Phys. Rev. A **8**, 3110 (1973).
[27] R. T. Farouki and S. Hamaguchi, Phys. Rev. E **47**, 4330 (1993).
[28] J. P. Schiffer, Phys. Rev. Lett. **88**, 205003 (2002).
[29] M. Drewsen, L. Hornekær, N. Kjærgaard, K. Mølhave, A. M. Thommesen, Z. Videsen, A. Mortensen, and F. Jensen, AIP Conference Proceedings 606, 135 (202).
[30] M. T. Bell, A. D. Gingell, J. Oldham, T. P. Softley, and S. Willitsch, Faraday Discuss. **142**, 73 (2009).
[31] C. B. Zhang, D. Offenberg, B. Roth, M. A. Wilson, and S. Schiller, Phys. Rev. A **76**, 012719 (2007).
[32] A. Steane, J. Phys. B: At. Mol. Opt. Phys. **64**, 623 (1997).
[33] D. F. V. James, Appl. Phys. B **66**, 181 (1998).
[34] G. Morigi and H. Walther, Eur. Phys. J. D **13**, 261 (2001).
[35] D. H. E. Dubin, Phys. Rev. Lett. **66**, 2076 (1991).
[36] D. H. E. Dubin, Phys. Rev. E **53**, 5268 (1996).
[37] T. B. Mitchell, J. J. Bollinger, X. P. Huang, and W. M. Itano, Opt. Express **2**, 314 (1998).
[38] A. Dantan, J. P. Marler, M. Albert, D. Guénot, and M. Drewsen, Phys. Rev. Lett. **105**, 103001 (2010).
[39] J. P. Schiffer, J. Phys. B: At. Mol. Opt. Phys. **36**, 511 (2003).
[40] E. S. Shuman, J. F. Barry, and D. DeMille, Nature **467**, 820 (2010).
[41] J. F. Barry, E. S. Shuman, E. B. Norrgard, and D. DeMille, arXiv: 1110.4890 [atomph] (2011).
[42] J. H. V. Nguyen, C. R. Viteri, E. G. Hohenstein, C. D. Sherrill, K. R. Brown, and B. Odom, New J. Phys. **13**, 063023 (2011).
[43] R. E. Drullinger, D. J. Wineland, and J. C. Bergquist, Appl. Phys. **22**, 365 (1980).
[44] D. J. Larson, J. C. Bergquist, J. J. Bollinger, W. M. Itano, and D. J. Wineland, Phys. Rev. Lett. **57**, 70 (1986).
[45] T. Baba and I. Waki, Jpn. J. Appl. Phys. **35**, 1134 (1996).
[46] K. Mølhave and M. Drewsen, Phys. Rev. A **62**, 011401 (2000).
[47] P. Bowe, L. Hornekaer, C. Brodersen, M. Drewsen, J. S. Hangst, and J. P. Schiffer, Phys. Rev. Lett. **82**, 2071 (1999).
[48] L. Hornekær, N. Kjærgaard, A. M. Thommesen, and M. Drewsen, Phys. Rev. Lett. **86**, 1994 (2001).
[49] B. Roth, P. Blythe, H. Wenz, H. Daerr, and S. Schiller, Phys. Rev. A **73**, 042712 (2006).
[50] B. Roth, P. Blythe, H. Daerr, L. Patacchini, and S. Schiller, J. Phys. B: At. Mol. Opt. Phys. **39**, S1241 (2006).

[51] X. Tong, A. H. Winney, and S. Willitsch, Phys. Rev. Lett. **105**, 143001 (2010).
[52] K. Højbjerre, D. Offenberg, C. Z. Bisgaard, H. Stapelfeldt, P. F. Staanum, A. Mortensen, and M. Drewsen, Phys. Rev. A **77**, 030702 (2008).
[53] A. Ostendorf, C. B. Zhang, M. A. Wilson, D. Offenberg, B. Roth, and S. Schiller, Phys. Rev. Lett. **97**, 243005 (2006).
[54] D. Offenberg, C. B. Zhang, Ch. Wellers, B. Roth, and S. Schiller, Phys. Rev. A **78**, 061401 (2008).
[55] D. Offenberg, Ch. Wellers, C. B. Zhang, B. Roth, and S. Schiller, J. Phys. B **42**, 035101 (2009).
[56] T. Baba and I. Waki, Appl. Phys. B **74**, 375 (2002).
[57] T. Baba and I. Waki, J. Appl. Phys. **92**, 4109 (2002).
[58] B. Roth, P. Blythe, and S. Schiller, Phys. Rev. A **75**, 023402 (2007).
[59] I. M. Buluta and S. Hasegawa, Phys. Rev. A **78**, 042340 (2008).
[60] I. M. Buluta and S. Hasegawa, J. Phys. B: At. Mol. Opt. Phys. **42**, 154004 (2009).
[61] N. Kimura, K. Okada, T. Takayanagi, M. Wada, S. Ohtani, and H. A. Schuessler, Phys. Rev. A **83**, 033422 (2011).
[62] K. Okada, K. Yasuda, T. Takayanagi, M. Wada, H. A. Schuessler, and S. Ohtani, Phys. Rev. A **75**, 033409 (2007).
[63] F. Calvo, C. Champenois, and E. Yurtsever, Phys. Rev. A **80**, 063401 (2009).
[64] C. Champenois, M. Marciante, J. Pedregosa-Gutierrez, M. Houssin, M. Knoop, and M. Kajita, Phys. Rev. A **81**, 043410 (2010).
[65] M. Marciante, C. Champenois, J. Pedregosa-Gutierrez, A. Calisti, and M. Knoop, Phys. Rev. A **83**, 021404 (2009).
[66] K. Okada, T. Takayanagi, M. Wada, S. Ohtani, and H. A. Schuessler, Phys. Rev. A **80**, 043405 (2009).
[67] I. M. Georgescu and S. Willitsch, Phys. Chem. Chem. Phys. **13**, 18852 (2011).
[68] D. Kielpinski, C. Monroe, and D. J. Wineland, Nature **417**, 709 (2002).
[69] D. Stick, W. K. Hensinger, S. Olmschenk, M. J. Madsen, K. Schwab, and C. Monroe, Nature Phys. **2**, 36 (2006).
[70] M. D. Hughes, B. Lekitsch, J. A. Broersma, and W. K. Hensinger, Contemporary Physics **52**, 505 (2011).
[71] J. M. Amini, J. Britton, D. Leibfried, and D. J. Wineland, in *Atom Chips*, edited by J. Reichel and V. Vuletić (Wiley-VCH, Weinheim, 2011), p. 395.
[72] J. Chiaverini, R. B. Blakestad, J. Britton, J. D. Jost, C. Langer, D. Leibfried, R. Ozeri, and D. J. Wineland, Quantum Inf. Comput. **5**, 419 (2005).
[73] A. Bertelsen, S. Jorgensen, and M. Drewsen, J. Phys. B: At. Mol. Opt. Phys. **39**, L83 (2006).
[74] J. C. J. Koelemeij, B. Roth, and S. Schiller, Phys. Rev. A **76**, 023413 (2007).
[75] X. Tong, D. Wild, and S. Willitsch, Phys. Rev. A **83**, 023415 (2011).
[76] R. Wester, J. Phys. B **42**, 154001 (2009).
[77] D. Gerlich and A. Borodi, Faraday Discuss. **142**, 57 (2009).
[78] I. S. Vogelius, L. B. Madsen, and M. Drewsen, Phys. Rev. Lett. **89**, 173003 (2002).
[79] I. S. Vogelius, L. B. Madsen, and M. Drewsen, J. Phys. B: At. Mol. Opt. Phys. **37**, 4571 (2004).
[80] I. S. Vogelius, L. B. Madsen, and M. Drewsen, J. Phys. B: At. Mol. Opt. Phys. **39**, S1267 (2006).
[81] I. S. Vogelius, L. B. Madsen, and M. Drewsen, J. Phys. B: At. Mol. Opt. Phys. **39**, S1259 (2006).
[82] P. F. Staanum, K. Højbjerre, P. S. Skyt, A. K. Hansen, and M. Drewsen, Nature Phys. **6**, 271 (2010).
[83] T. Schneider, B. Roth, H. Duncker, I. Ernsting, and S. Schiller, Nature Phys. **6**, 275 (2010).
[84] S. Willitsch, Nature Phys. **6**, 240 (2010).
[85] S. Willitsch and F. Merkt, Int. J. Mass Spectrom. **245**, 14 (2005).
[86] S. R. Mackenzie, F. Merkt, E. J. Halse, and T. P. Softley, Mol. Phys. **86**, 1283 (1995).
[87] S. Schlemmer, T. Kuhn, E. Lescop, and D. Gerlich, Int. J. Mass Spectrom. **185/186/187**, 589 (1999).

[88] C. Lazarou, M. Keller, and B. M. Garraway, Phys. Rev. A **81**, 013418 (2010).
[89] S. Ding and D. N. Matsukevich, arXiv: 1109.4251 [quant-ph] (2011).
[90] D. Leibfried, arXiv: 1109.0208 [quant-ph] (2011).
[91] T. Baba and I. Waki, J. Chem. Phys. **116**, 1858 (2002).
[92] M. Drewsen, A. Mortensen, R. Martinussen, P. Staanum, and J. L. Sorensen, Phys. Rev. Lett. **93**, 243201 (2004).
[93] P. F. Staanum, K. Højbjerre, and M. Drewsen, in *Practical Aspects of Trapped Ion Mass Spectrometry*, edited by Raymond E. March and John F. Todd (Vol. 5, CRC Press, Boca Raton, 2010), p. 291.
[94] P. F. Staanum, K. Højbjerre, R. Wester, and M. Drewsen, Phys. Rev. Lett. **100**, 243003 (2008).
[95] R. V. Krems, Phys. Chem. Chem. Phys. **10**, 4079 (2008).
[96] M. T. Bell and T. P. Softley, Mol. Phys. **107**, 99 (2009).
[97] O. Dulieu, R. Krems, M. Weidemüller, and S. Willitsch, Phys. Chem. Chem. Phys. **13**, 18703 (2011).
[98] K. K. Ni, S. Ospelkaus, D. Wang, G. Quéméner, B. Neyenhuis, M. H. G. de Miranda, J. L. Bohn, J. Ye, and D. S. Jin, Nature **464**, 1324 (2010).
[99] M. H. G. de Miranda, A. Chotia, B. Neyenhuis, D. Wang, G. Qéméner, S. Ospelkaus, J. L. Bohn, J. Ye, and D. S. Jin, Nature Phys. **7**, 502 (2011).
[100] S. Ospelkaus, K. K. Ni, D. Wang, M. H. G. de Miranda, B. Neyenhuis, G. Quéméner, P. S. Julienne, J. L. Bohn, D. S. Jin, and J. Ye, Science **327**, 853 (2010).
[101] S. Knoop, F. Ferlaino, M. Berninger, M. Mark, H. C. Nägerl, R. Grimm, J. P. D'Incao, and B. D. Esry, Phys. Rev. Lett. **104**, 053201 (2010).
[102] J. J. Gilijamse, S. Hoekstra, S. Y. T. van de Meerakker, G. C. Groenenboom, and G. Meijer, Science **313**, 1617 (2006).
[103] M. Kirste, L. Scharfenberg, Kłos J., F. Lique, M. H. Alexander, G. Meijer, and S. Y. T. van de Meerakker, Phys. Rev. A **82**, 042717 (2010).
[104] L. Scharfenberg, J. Kłos, P. J. Dagdigian, M. H. Alexander, G. Meijer, and S. Y. T. van de Meerakker, Phys. Chem. Chem. Phys. **12**, 10660 (2010).
[105] S. Willitsch, M. T. Bell, A. D. Gingell, S. R. Procter, and T. P. Softley, Phys. Rev. Lett. **100**, 043203 (2008).
[106] B. Gao, Phys. Rev. Lett. **104**, 213201 (2010).
[107] B. Gao, Phys. Rev. A **83**, 062712 (2011).
[108] E. I. Dashevskaya, A. I. Maergoiz, J. Troe, I. Litvin, and E. E. Nikitin, J. Chem. Phys. **118**, 7313 (2003).
[109] P. B. Armentrout, J. Anal. At. Spectrom. **19**, 571 (2004).
[110] I. W. M. Smith, Angew. Chem. Int. Ed. **45**, 2842 (2006).
[111] D. C. Clary, Chem. Phys. Lett. **232**, 267 (1995).
[112] R. Côté and A. Dalgarno, Phys. Rev. A **62**, 012709 (2000).
[113] S. Bovino, M. Tacconi, and F. A. Gianturco, J. Phys. Chem. A **115**, 8197 (2011).
[114] Z. Idziaszek, A. Simoni, T. Calarco, and P. S. Julienne, New J. Phys. **13**, 083005 (2011).
[115] L. D. Carr, D. DeMille, R. V. Krems, and J. Ye, New J. Phys. **11**, 055049 (2009).
[116] M. Schnell and G. Meijer, Angew. Chem. Int. Ed. **48**, 6010 (2009).
[117] J. Deiglmayr, A. Grochola, M. Repp, K. Mörtlbauer, C. Glück, J. Lange, O. Dulieu, R. Wester, and M. Weidemüller, Phys. Rev. Lett. **101**, 133004 (2008).
[118] K. K. Ni, S. Ospelkaus, M. H. G. de Miranda, A. Pe'er, B. Neyenhuis, J. J. Zirbel, S. Kotochigova, P. S. Julienne, D. S. Jin, and J. Ye, Science **322**, 231 (2008).
[119] M. Vitteau, A. Chotia, M. Allegrini, N. Bouloufa, O. Dulieu, D. Comparat, and P. Pillet, Science **321**, 232 (2008).
[120] J. G. Danzl, M. J. Mark, E. Haller, M. Gustavsson, R. Hart, J. Aldegunde, J. M. Hutson, and H. C. Nägerl, Nature Phys. **6**, 265 (2010).

[121] S. A. Rangwala, T. Junglen, T. Rieger, P. W. H. Pinkse, and G. Rempe, Phys. Rev. A **67**, 043406 (2003).
[122] A. D. Gingell, M. T. Bell, J. M. Oldham, T. P. Softley, and J. M. Harvey, J. Chem. Phys. **133**, 194302 (2010).
[123] R. Côté, V. Kharchenko, and M. D. Lukin, Phys. Rev. Lett. **89**, 093001 (2002).
[124] C. Zipkes, S. Palzer, L. Ratschbacher, C. Sias, and M. Köhl, Phys. Rev. Lett. **105**, 133201 (2010).
[125] S. Schmid, A. Härter, and J. Hecker Denschlag, Phys. Rev. Lett. **105**, 133202 (2010).
[126] A. Rakshit and B. Deb, Phys. Rev. A **83**, 022703 (2011).
[127] E. R. Hudson, Phys. Rev. A **79**, 032716 (2009).
[128] C. Zipkes, S. Palzer, C. Sias, and M. Köhl, Nature **464**, 388 (2010).
[129] R. Côté, Phys. Rev. Lett. **85**, 5316 (2000).
[130] O. P. Makarov, R. Côté, H. Michels, and W. W. Smith, Phys. Rev. A **67**, 042705 (2003).
[131] W. W. Smith, O. P. Makarov, and J. Lin, J. Mod. Opt. **52**, 2253 (2005).
[132] M. Cetina, A. Grier, J. Campbell, I. Chuang, and V. Vuletic, Phys. Rev. A **76**, 041401 (2007).
[133] A. T. Grier, M. Cetina, F. Oručević, and V. Vuletić, Phys. Rev. Lett. **102**, 223201 (2009).
[134] K. Ravi, A. Sharma, G. Werth, and S. A. Rangwala, Appl. Phys. B. [online], DOI 10.1007/s00340–011–4726–6 (2011).
[135] W. G. Rellergert, S. T. Sullivan, S. Kotochigova, A. Petrov, K. Chen, S. J. Schowalter, and E. R. Hudson, Phys. Rev. Lett. **107**, 243201 (2011).
[136] F. H. J. Hall, M. Aymar, N. Bouloufa-Maafa, O. Dulieu, and S. Willitsch, Phys. Rev. Lett. **107**, 243202 (2011).
[137] E. L. Raab, M. Prentiss, A. Cable, S. Chu, and D. E. Pritchard, Phys. Rev. Lett. **59**, 2631 (1987).
[138] P. Zhang, A. Dalgarno, and R. Côté, Phys. Rev. A **80**, 030703 (2009).
[139] J. Weiner, V. S. Bagnato, S. Zilio, and P. S. Julienne, Rev. Mod. Phys. **71**, 1 (1999).
[140] S. Schiller and V. Korobov, Phys. Rev. A **71**, 032505 (2005).
[141] T. Rosenband, D. B. Hume, P. O. Schmidt, C. W. Chou, A. Brusch, L. Lorini, W. H. Oskay, R. E. Drullinger, T. M. Fortier, J. E. Stalnaker, S. A. Diddams, and W. C. Swann, Science **319**, 1808 (2008).
[142] D. Bakalov, V. Korobov, and S. Schiller, Phys. Rev. A **82**, 055401 (2010).
[143] M. G. Kozlov and S. A. Levshakov, Astrophys. J. **726**, 65 (2011).
[144] K. Beloy, M. G. Kozlov, A. Borschevsky, A. W. Hauser, V. V. Flambaum, and P. Schwerdtfeger, Phys. Rev. A **83**, 062514 (2011).
[145] A. E. Leanhardt, J. L. Bohn, H. Loh, P. Maletinsky, E. R. Meyer, L. C. Sinclair, R. P. Stutz, and E. A. Cornell, J. Mol. Spectrosc. **270**, 1 (2011).
[146] J. J. Hudson, D. M. Kara, I. J. Sallman, B. E. Sauer, M. R. Tarbutt, and E. A. Hinds, Nature **473**, 493 (2011).
[147] M. Schnell and J. Küpper, Faraday Discuss. **150**, 33 (2011).
[148] B. Roth, J. C. J. Koelemeij, H. Daerr, and S. Schiller, Phys. Rev. A **74**, 040501 (2006).
[149] J. C. J. Koelemeij, B. Roth, A. Wicht, I. Ernsting, and S. Schiller, Phys. Rev. Lett. **98**, 173002 (2007).
[150] S. Bize, S. A. Diddams, U. Tanaka, C. E. Tanner, W. H. Oskay, R. E. Drullinger, T. E. Parker, T. P. Heavner, S. R. Jefferts, L. Hollberg, W. M. Itano, and J. C. Bergquist, Phys. Rev. Lett. **90**, 150802 (2003).
[151] H. Häffner, C. F. Roos, and R. Blatt, Phys. Rep. **469**, 155 (2008).
[152] P. O. Schmidt, T. Rosenbrand, C. Langer, W. M. Itano, J. C. Bergquist, and D. J. Wineland, Science **309**, 749 (2005).

[153] P. O. Schmidt, T. Rosenband, J. C. J. Koelemeij, D. B. Hume, W. M. Itano, J. C. Bergquist, and D. J. Wineland, in *AIP Conference Proceedings*, edited by M. Drewsen, U. Uggerhoj, and H. Knudsen, Vol. CP862 (American Institute of Physics, Melville, 2006), p. 305.
[154] J. Mur-Petit, J. J. Garcia-Ripoll, J. Pérez-Ríos, J. Campos-Martínez, M. I. Hernández, and S. Willitsch, Phys. Rev. A **85**, 022308 (2012).